Comparison of Two Linear Models for Estimating Brain Deformation during Surgery Using Finite Element Method

Hajar Hamidian, Hamid Soltanian-Zadeh, Reza Faraji-Dana, and Masoumeh Gity

Abstract— **This paper presents finite element computation of brain deformation during craniotomy. Two mechanical models are compared for this purpose: linear solid-mechanic model and linear elastic model. Both models assume finite deformation of the brain after opening the skull. We use a test sphere as a model of the brain, tetrahedral finite element mesh, and function optimization that optimizes the models' parameters by minimizing the distance between the resulting deformation and the supposed deformation. Based on the final value of the objective function, we conclude that the accuracy of the solid mechanic model is higher than that of the elastic model. Applications of the methods to the MR images of the brain confirm this finding.**

I. INTRODUCTION

MECHANICAL property of very soft tissue such as brain, has been studied in recent years for applications like surgical planning [1]. However, in a common neurosurgical procedure the brain deforms after opening the skull, causing misalignment of the subject to the preoperative images [2], [3] (Figure 1). This happens because of cerebrospinal fluid (CSF) leakage, dura opening, anaesthetics and osmotic agents, as well as conditions which are different from the normal state [4], [5]. While the intraoperative imaging such as iMRI is the best way to determine this deformation, intraoperative images suffer from the constraints of the operating room [6]. This problem can be avoided by using biomedical models.

In this paper, two models are used as described next. The first model is based on the biphasic soft-tissue [7] that assumes the brain tissue behaves as a linear elastic material and indicates that the stress can be related to strain by Hook's law [8], [9]. The second model is based on the principle that the sum of the virtual work from the internal strains is equal to the work from the external loads [10], [11]. In most practical cases, such models utilize the finite element methods [12] to solve sets of partial differential equations governing the deformation behavior of the tissue. For solving these models, we must know the value of the brain' s parameters. Previous works used approximate values of the brain parameters, which we also use in this work as initial values. We apply function optimization to optimize these parameters and minimize the distance between the resulting points and the supposed points.

We use the above two models of the brain and optimize their parameters to match the resulting deformation with the assumed deformation. We then compare the two models using their resulting errors on the simulated model and real brain images. In the next section, we explain the models and describe how to use meshing and boundary conditions for solving the problem using finite element methods and how to use function optimization to optimize their parameters. In Section III, we explain the results of our implementation on a sphere and real brain extracted from MRI. Section IV presents the conclusions of our work.

Manuscript received December 31, 2008. This work was supported in part by the University of Tehran, School of Electrical and Computer Engineering.

Hajar Hamidian is with the Control and Intelligent Processing Center of Excellence (CIPCE), School of Electrical and Computer Engineering, University of Tehran, Tehran, Iran. Phone: (+98-21) 6111-4173; Fax: (+98-21) 8877-8690; E-mail: h.hamidian@ece.ut.ac.ir.

Hamid Soltanian Zadeh is with the Control and Intelligent Processing Center of Excellence (CIPCE), School of Electrical and Computer Engineering, University of Tehran, Tehran, Iran and the Radiology Image Analysis Lab., Henry Ford Hospital, Detroit, MI 48202, USA. E-mails: hszadeh@ut.ac.ir, hamids@rad.hfh.edu.

Reza Faraji-Dana is with the School of Electrical and Computer Engineering, University of Tehran, Tehran, Iran. E-mail: reza@ut.ac.ir.

Masoumeh Gity is the Department of Radiology, University of Tehran Medical School, Tehran, Iran. E-mail: p_gity@yahoo.com.

II. MATERIALS AND METHODS

A. Construction of Finite Element Mesh

Within Finite Element Modeling (FEM) framework, the body on which one is working needs to be discretized using finite element mesh. To this end, we used a sphere with a diameter of 22 Cm which is approximately the size of the brain. We also use COMSOL3.3 software which is based on the finite element methods for solving partial differential equations, visualization, and meshing. It also has strong post processing modules to generate 4-noded tetrahedral mesh with Lagrange shape function (Figure 2). An example of the mesh generated by the software is shown in Figure 2 which consists of 10,164 tetrahedral elements.

B. The Computational Biomedical Models

As mentioned in section I, for determining the deformation of the brain, a model of the brain may be used. Such a model provides numerical formulation that describes the behavior of the brain tissue. These formulations can be linear or non-linear [13], [14]. In this paper, we use and compare two models that describe the tissue behavior linearly.

978-1-4244-1821-3/08/$25.00©2008 IEEE

TABLE I
PARAMETER USED IN EQUATION (4), (5)

Parameter symbol	Description	Value
E	Young modulus	2100 Pa
υ	Poisson's ratio	0.45
ρ_t	Density of brain tissue	1000 kg/m^3
ρ_f	Density of surrounding tissue	1000 kg/m^3
K	Hydraulic conductivity	1e-7m^{3}s/kg
α	Ratio of fluid volume extracted to volume change of the tissue under compression	1
1/S	Amount of fluid which can be forced into the tissue under constant volume	0
Ψ	Magnetic dipole moment	0.001 Pa/s
G	Shear modulus	E/2(υ+1) Pa

1) Linear Solid-Mechanic Model

In this model, the body is assumed to be a linear elastic continuum with no initial stresses or strains. The energy of the body' s deformation caused by externally applied forces can be expressed as equation (1) [10].

$$E = \frac{1}{2}\int_{\Omega} \sigma^T \varepsilon \, d\Omega + \int_{\Omega} F^T u d\Omega, \qquad (1)$$

Where $F = F(x,y,z)$ is the total force applied to the elastic body, Ω is the elastic body, u is the displacement vector, and ε is the strain vector that can be defined as equation (2) [10].

$$\varepsilon = (\frac{\partial u}{\partial x}, \frac{\partial u}{\partial y}, \frac{\partial u}{\partial z}, \frac{\partial u}{\partial x} + \frac{\partial u}{\partial y}, \frac{\partial u}{\partial y} + \frac{\partial u}{\partial z}, \frac{\partial u}{\partial x} + \frac{\partial u}{\partial z})^T = Lu \qquad (2)$$

Also, σ is the stress vector and in the case of linear elasticity, with no initial stresses or strains, relates to the strain vector by the linear equation $\sigma = D\varepsilon$ where D is the elasticity matrix describing the material properties [10]. The value of D depends on two material parameters: the Young modules and the Poisson ratios. Volumetric deformation of the brain is founded by solving equation (1) for the displacement vector u, which minimizes the energy function E. The solution to these equations can be written in a global linear equation (3) [11].

$$Ku = -F \qquad (3)$$

The solution of equation (3) provides the deformation field that results from the forces applied to the body. We rely on the study of Ferrant *et al* in [10] and choose our initial coefficients (Young modules = 3 kPa, Poisson ratio = 0.45).

2) Linear Elastic Model

This model assumes that the deformation of the brain tissue as a poroelastic material occurs because of its elastic behavior and the pressure of exteracellular fluid [12]. The important body forces that affect the brain deformation are the gravity, ($\rho_t g$), where ρ_t is the density of the brain, the buoyancy of the surrounding fluid ($\rho_f g$), where ρ_f is the density of the surrounding fluid, and the pressure gradient of the exteracellular fluid (∇p). Based on these assumptions, the model can be written as equation (4) [15].

$$\nabla . G\nabla u + \nabla \frac{G}{1-2\upsilon}(\nabla . u) - \alpha \nabla p = (\rho_t - \rho_f) g \qquad (4)$$

where G is the shear modulus, υ is the Poisson' s ratio, u is the displacement vector, p is the pore fluid pressure, and ∇p is the ratio of fluid volume extracted to deform the tissue under compression. Equation (4) relates the mechanical property of the tissue to the gradient of fluid pressure across the medium. This equation considers three scalar equations involving four dependant variables: u_x, u_y, u_z, and p. For solving the problem, we need the equation that relates the deformation of the tissue to the exiting of the fluid after the craniotomy. This can be described as equation

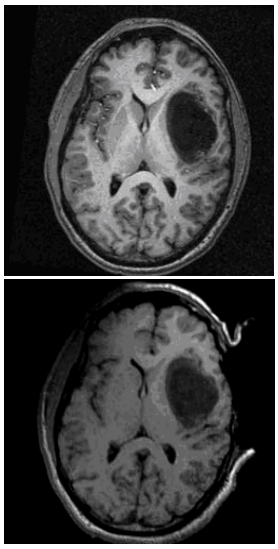

Figure 1. MRI images a) before opening the skull, b) after opening the skull.

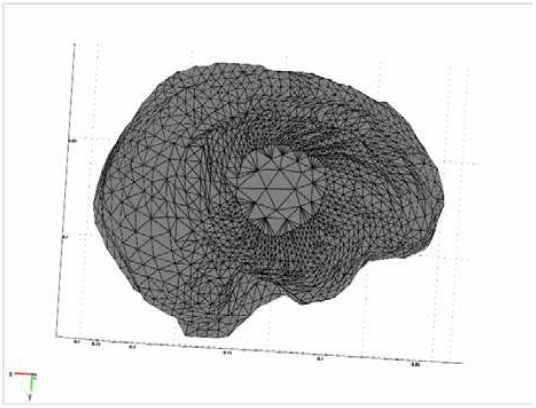

Figure 2. The result of meshing a brain volume.

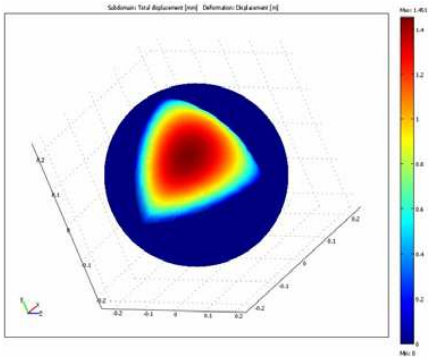

Figure 3. Result of the first model.

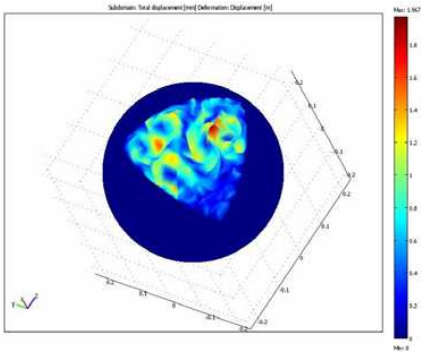

Figure 4. Result of the second model.

(5) [16].

$$\alpha \frac{\partial}{\partial t}(\nabla .u) - \nabla .k\nabla p + \frac{1}{S}\frac{\partial p}{\partial t} = \Psi \qquad (5)$$

where k is hydraulic conductivity, $1/S$ is the amount of fluid that can be forced into the tissue under constant volume, and Ψ is the pressure source strength. The initial values of the parameters are given in Table I.

These equations describe the behavior of the brain' s tissue as linear elastic material and the pore fluid as incompressible material. Generally, the brain can be modeled as a saturated material thus omitting the derivation of the pressure with respect to time in equation (5) (i.e., $\alpha = 1, 1/S = 0$). This model allows accessing more elastic boundary conditions of the intracranial pressure by modeling CSF drainage while maintaining linearity. That is an important computational advantage.

C. Boundary Conditions

We need boundary conditions to solve the equations. In this paper, for testing of the methods, we use a sphere as a simple model of the brain and expose a section of it. In this case, the exposed section would be free and the rest of the model would be fixed.

For the first model, we have conditions for the displacement variable and force per unit (F). We use $F=u$ for the boundary conditions of the fixed boundary nodes because the elements of the rigidity matrix K in equation (3) that the deformation is supposed to be known need to be set to zero, and the diagonal elements of these rows to one. More details can be found in [10]. For the exposed surface, we assume the center of this boundary to be constant and the value for the rest will be free to change. The initial value of this parameter is defined by examination of the MR images of six different patients.

For the second model, the boundary condition for p rather than displacement variable is needed. The corresponding nodes in the mesh lying above the level of intra-operative CSF drainage are assumed to reside at atmospheric pressure (Dirichlet condition in pressure), while those that do not, are the non-draining regions of the brain (Neumann condition in pressure).

D. The Optimization Process

The parameters of the brain in each model are not the same for different patients and thus usually approximated parameters are used. In this paper, we use an optimization process to optimize these parameters and achieve most accurate results with respect to the pre-defined deformations. To this end, we choose a cost function defined as the sum of the distances between the defined points and the resulting points. We use the Maltlab optimization toolbox for the optimization procedure.

Displacements of specific points can be determined by an expert or an imaging device such as MRI, CT, or spectroscopic camera. In this paper, we use 10 points of a sphere in the optimization process and another 10 points for testing of the results.

In both methods, we have some parameters to optimize. In the first model, we cannot determine the force applied to the exposed surface of the brain. This parameter can be defined by the optimization process. Two parameters (Young modulus and Poisson's ratio) are reported in the literature but they are not the same for different patients and thus they will be optimized. In the second model, the parameters in Table I except for $\alpha, 1/S$ are used as the optimization parameters. We determine the brain' s deformation in the steady state which means that we don not consider the transient changing of p in equation (5) and thus Ψ / k is used for the optimization process.

III. RESULTS

For modeling the brain, we have used a sphere with the diameter of 22 Cm which is approximately the size of the brain. To show the skull opening, we have assumed that one section of this sphere is exposed and other sections are fixed. We have assumed a model with specific parameters and have specified the deformation of specific points to use in the optimization process and some other points for the testing of the optimization process. Then, we have changed the parameters and have used the optimization process to

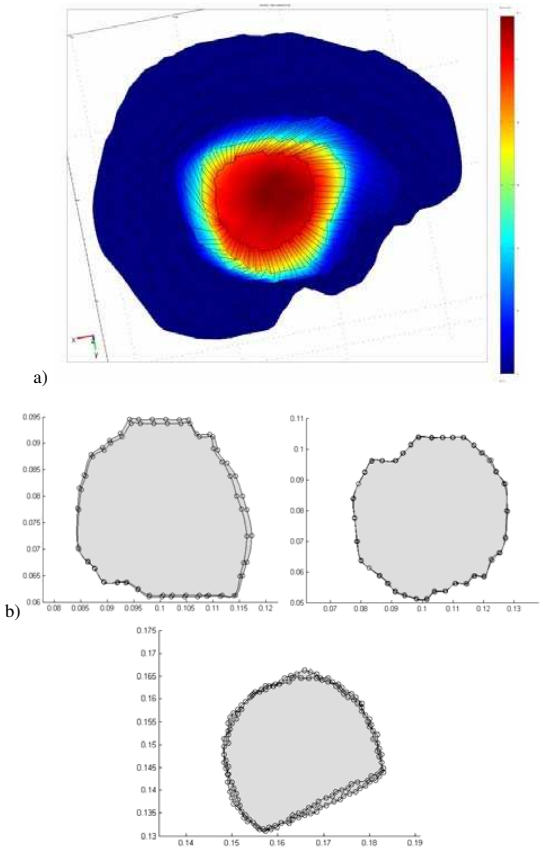

Figure 5. Result of the first model, a) 3D result for brain, b) 2D result for tumor.

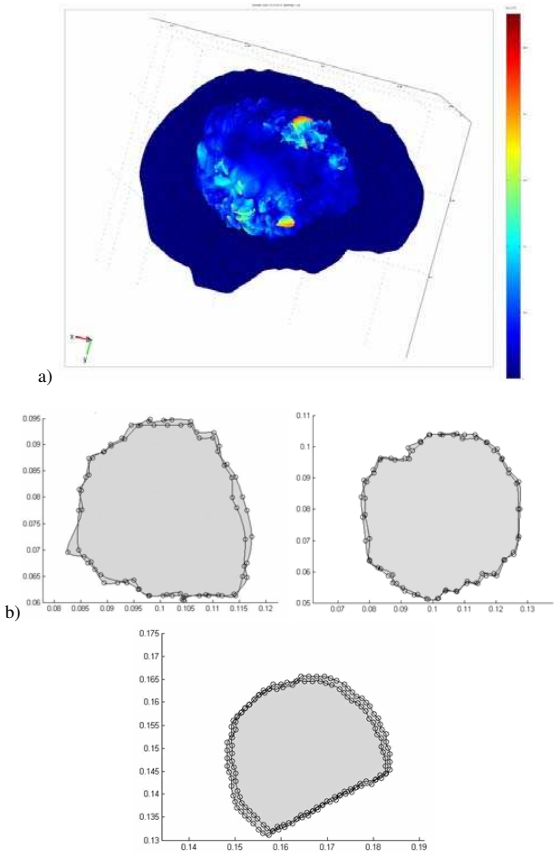

Figure 6. Result of the second model, a) 3D result for brain, b) 2D result for tumor.

estimate the assumed model' s parameters by using displacement of points in the assumed model. This can show us if the deformation of the brain can be modeled with a specific model and if our proposed method can accurately estimate that model. For each model, we have done this process and have compared the accuracy of models using error of the optimization function and the error of displacement for other points that we did not use in the optimization process. To implement the models, we use the COMSOL3.3 software which is based on the finite element methods for solving partial differential equations.

Figures 3-4 show the results of the first and second models for the sphere. As seen, the deformation of the first model is more similar to the brain deformation because its deformation is continuous. The results of the second model have some outstanding points and the deformation is not smooth. In addition, in the first model, the mean and maximum error of the points used in the optimization process are 0.1172 mm and 0.4123 mm respectively, and the mean and maximum error of the points that are not used in the optimization process is 0.2731 mm and 0.5836 mm respectively. For the second model, these values are 0.1915 mm, 0.5214 mm, 0.3215 mm, and 0.7198 respectively. Therefore, accuracy of the first model is higher than the second model. Tables II-III show the assumed and estimated parameters for the two models.

To find optimal estimates of the parameters, we should consider the tolerance of the parameters with respect to the initial values and how much the model is sensitive to the variations of the parameters. As can be seen, the optimization process estimates the Young modulus and Poisson's ratio for the first model better than the second model. In addition, the second model is very sensitive to the variation of the parameter $\rho_t - \rho_f$ and a little change can affect the result of model more compared to the variations of the F parameter in the first model. Also, the optimization process optimizes the F parameters better than Ψ / k. The sensitivity of the first model to the F parameter is approximately equal to the sensitivity of the second model to the Ψ / k parameter. Thus, the optimization process can estimate the parameters of the first model more accurately than the second model.

TABLE II
ASSUMED AND ESTIMATED PARAMETERS FOR THE FIRST MODEL.

	Young modulus	Poisson's ratio	Force
Assumed	0.45	3000	Fx=1500 Fy=1500 Fz=1500
Estimated	0.45 ± 0.0056	3000 ± 175	Fx=1500 ± 90 Fy=1500 ± 87 Fz=1500 ± 93

TABLE III
ASSUMED AND ESTIMATED PARAMETERS FOR THE SECOND MODEL.

	E	ν	ρ_t	ρ_f	Ψ/k
Assumed	2100	0.45	1000	1000	1.01e4
Estimated	2100 ±195	0.45 ± 0.07	1000 ± 60	1000 ± 40	1.01e4 ± 800

TABLE IV
THE TOLERANCE OF THE MAXIMUM AND MEAN ERROR FOR THE TESTING LANDMARKS

	Case 1	Case 2	Case 3	Case 4	Case 5	Case 6
Max error for mechanical model	$\Delta x = 3.0mm$ $\Delta y = 3.3mm$ $\Delta z = 1.1mm$	$\Delta x = 3.3mm$ $\Delta y = 3.2mm$ $\Delta z = 0.1mm$	$\Delta x = 3.4mm$ $\Delta y = 4.4mm$ $\Delta z = 0.3mm$	$\Delta x = 2.9mm$ $\Delta y = 3.1mm$ $\Delta z = 0.8mm$	$\Delta x = 2.7mm$ $\Delta y = 2.8mm$ $\Delta z = 0.4mm$	$\Delta x = 4.0mm$ $\Delta y = 3.4mm$ $\Delta z = 1.7mm$
Mean error for mechanical model	$\Delta x = 1.2mm$ $\Delta y = 1.2mm$ $\Delta z = 0.4mm$	$\Delta x = 1.3mm$ $\Delta y = 1.0mm$ $\Delta z = 0.3mm$	$\Delta x = 1.3mm$ $\Delta y = 1.7mm$ $\Delta z = 0.1mm$	$\Delta x = 0.9mm$ $\Delta y = 1.1\ mm$ $\Delta z = 0.5\ mm$	$\Delta x = 0.9mm$ $\Delta y = 0.8mm$ $\Delta z = 0.1\ mm$	$\Delta x = 1.0mm$ $\Delta y = 0.7mm$ $\Delta z = 0.1mm$
Max error for elastic model	$\Delta x = 4.1mm$ $\Delta y = 3.9mm$ $\Delta z = 1.4mm$	$\Delta x = 3.9mm$ $\Delta y = 3.6mm$ $\Delta z = 1.2mm$	$\Delta x = 3.8mm$ $\Delta y = 4.4mm$ $\Delta z = 0.4mm$	$\Delta x = 3.1mm$ $\Delta y = 3.2mm$ $\Delta z = 1.04mm$	$\Delta x = 3.0mm$ $\Delta y = 2.9mm$ $\Delta z = 0.7mm$	$\Delta x = 3.5mm$ $\Delta y = 4.1mm$ $\Delta z = 1.3mm$
Mean error for elastic model	$\Delta x = 1.8mm$ $\Delta y = 1.4mm$ $\Delta z = 0.5mm$	$\Delta x = 1.7mm$ $\Delta y = 1.2mm$ $\Delta z = 0.5mm$	$\Delta x = 1.4mm$ $\Delta y = 1.8mm$ $\Delta z = 0.2mm$	$\Delta x = 1.2mm$ $\Delta y = 1.5mm$ $\Delta z = 0.6mm$	$\Delta x = 1.0mm$ $\Delta y = 1.2mm$ $\Delta z = 0.4mm$	$\Delta x = 1.1mm$ $\Delta y = 1.2mm$ $\Delta z = 0.2mm$

To evaluate the methods on the real data, we have used six pre-operative and post-operative MRI studies of different patients undergoing brain tumor surgery. The pre-operative and intra-operative images have been registered rigidly using ITK, and then anatomical landmarks have been determined by our expert radiologist in the pre- and intra-operative images. For each patient study, the expert has selected about 60 pairs of corresponding landmarks. One half of the landmarks have been used in the optimization process and the other half have been used for testing of the methods. The brain and the tumor have been segmented using the 3D-Slicer software and 3D models of the brain and the tumor have been created using the COMSOL3.3 software. For generating the models we use the initial value of parameters used in the simulation model. For mesh generation and numerically solving the models equations, we have used the COMSOL3.3 software. For the optimization process, we have used the MATLAB optimization toolbox. By comparing the matching error of the training landmarks and that of the testing landmarks, capability of each model for accurate estimation of the brain deformations has been evaluated.

The tolerance of the maximum and mean error for the testing landmarks in six cases are presented in Table IV. The testing landmarks are mostly near the exposed surface and the accuracy of both models is acceptable for them. However, the accuracy of the first model in terms of both the maximum and the mean error is superior to the second model in most cases. Figure 5-6 show the results of the two models on MR images of the brain in two and three dimensions. Note that the results of both models show good matching for the tumor in two dimensions in comparison with the intra-operative tumor images but the first model offers superior results. This can be seen in larger scale better. These results are consistent with the results of the sphere simulation study.

IV. CONCLUSION

In estimating the brain deformations, model selection is an important step for obtaining valid results. To this end, we studied two linear mechanical models for describing the mechanical properties of the brain tissue based on finite deformation and implemented them on a simple sphere and real models of the brain extracted from MRI. The first model is based on the virtual works applied to the inside and outside of the brain but the second model is based on the equations that relate the displacement of the volume to the pressure of the fluid. The first model generated shape deformations similar to the brain deformations and its application to a sphere generated more accurate displacements than the second model. Also, applications of the two models to the real data resulted in good matching of the tumor in the two dimensions but the first model generated superior results.

ACKNOWLEGEMENT

The patient-specific geometric data for the brain were obtained from pre- and intra-operative MRIs of six different patients undergoing brain tumor surgery at the Surgical Planning Laboratory, Brigham and Women's Hospital (Harvard Medical School, Boston, Massachusetts, USA). The authors gratefully acknowledge and thank Dr. Ron Kikinis and Dr. Tina Kapur for providing this data.

REFERENCES

[1] A. Wittek, K. Miller, J. Laporte, R. Kikinis, S. Warfield, "Computing reaction forces on surgical tools for robotic neurosurgery and surgical simulation," *CD Proceedings of Australasian Conference on Robotics and Automation ACRA. Canberra*, Australia, 2004.

[2] K. Miller, "Method of testing very soft biological tissues in compression," *J. Biomechanics*, vol. 38, pp.153–158, 2005.

[3] M. I. Miga, K. D. Paulsen, P. J. Hoopes, F. E. Kennedy, J. A. Hartov, and D. W. Roberts, "In Vivo quantification of a homogeneous brain deformation model for updating preoperative images during surgery," *IEEE Trans. Biomed. Eng*., vol. 47, no. 2, pp. 266-273, Feb. 2000.

[4] P. Dumpuri, R. C. Thompson, B. M. Dawant, A. Cao, M. I. Miga, "An atlas-based method to compensate for brain shift: Preliminary results," *Medical Image Analysis*, vol. 11, pp. 128–145, 2007.

[5] L. A. Platenik, M. I. Miga, D. W. Roberts, K. E. Lunn, F. E. Kennedy, A. Hartov, and K. D. Paulsen, "In vivo quantification of retraction deformation modeling for updated image-guidance during neurosurgery," *IEEE Trans. Biomed. Eng*., vol. 49, no. 8, pp. 823-835, Aug. 2002.

[6] Clatz, H. Delingette, I. F. Talos, A. J. Golby, R. Kikinis, F. A. Jolesz, N. Ayache, and S. K. Warfield, "Robust nonrigid registration to capture brain shift from intraoperative MRI," *IEEE Trans. Med. Imag.*, vol. 24, no. 11, pp. 1417-1427, Nov. 2005.

[7] K. D. Paulsen, M. I. Miga, F. E. Kennedy, P. J. Hoopes, A. Hartov, and D. W. Roberts, "A computational model for tracking subsurface tissue deformation during stereotactic neurosurgery," *IEEE Trans. Biomed. Eng*., vol. 46, no. 2, Feb. 1999.

[8] K. D. Paulsen, M. I. Miga, D. W. Roberts, F. E. Kennedy, L. A. Platenik, K. E. Lunn, and A. Hartov, "Finite element modeling of tissue retraction and resection for preoperative neuroimage compension with surgery," *Medical Imaging 2001: Visualization, Display, and Image-guided Procedures,* vol. 2, no. 24, pp. 13-21, 2001.

[9] M. I. Miga, T. K. Sinha, D. M. Cash, R. L. Galloway, and R. J. Weil, "Cortical surface registration for image-guided neurosurgery using laser-range scanning," *IEEE Trans. Med. Imag.*, vol. 22, no. 8, pp. 973–985, Aug. 2003.

[10] M. Ferrant, A. Nabavi, B. Macq, P. M. Black, F. A. Jolesz , R. Kikinis, and S. K. Warfield, "Serial registration of intraoperative MR images of the brain," *Med. Imag. Analysis*, vol. 6, p.p. 337–359, 2002.

[11] M. Ferrant, A. Nabavi, B. Macq, F. A. Jolesz, R. Kikinis, S. K. Warfield, "Registration of 3-D intraoperative MR images of the brain using a finite element biomechanical model," *IEEE Trans. Med. Imag.*, vol. 20, pp.1384–1397, 2001.

[12] K. J. Bathe, "Finite element procedures," *Prentice-Hall*, Englewood Cliffs, NJ. 1996.

[13] Wittek, K. Miller, R. Kikinis, S. K. Warfield, "Patient-specific model of brain deformation: Application to medical image registration," *J. Biomech.,* in press, Accepted 27 February 2006.

[14] A. Wittek, R. Kikinis, S. K. Warfield, and K. Miller, "Computation using a fully nonlinear biomechanical model," *in proc. of MICCAI 2005, LNCS, Springer-Verlag, Berlin Heidelberg*, vol. 3750, pp. 583 – 590, 2005.

[15] M. I. Miga, K. D. Paulsen, J. M. Lemery, S. D. Eisner, A. Hartov, F. E. Kennedy, and D. W**.** Roberts, "Model-Updated Image Guidance: Initial clinical experiences with gravity-induced brain deformation," *IEEE Tran. Med. Imag***.,** vol. 18, no. 10, Oct. 1999.

[16] K. E. Lunn, K. D. Paulsen, F. Liu, F. E. Kennedy, A. Hartov, and D. W. Roberts, "Data-guided brain deformation modeling: evaluation of a 3-D adjoint inversion method in porcine studies," *IEEE Trans. Biomed. Eng*., vol. 53, no. 10, pp. 1893-1900, Oct. 2006.